IEEE Photonics Journal
An IEEE Photonics Society Publication

Open Access

Precise Brightfield Localization Alignment for Fourier Ptychographic Microscopy

Volume 10, Number 1, February 2018

Jizhou Zhang
Tingfa Xu
Jingdan Liu
Sining Chen
Xing Wang

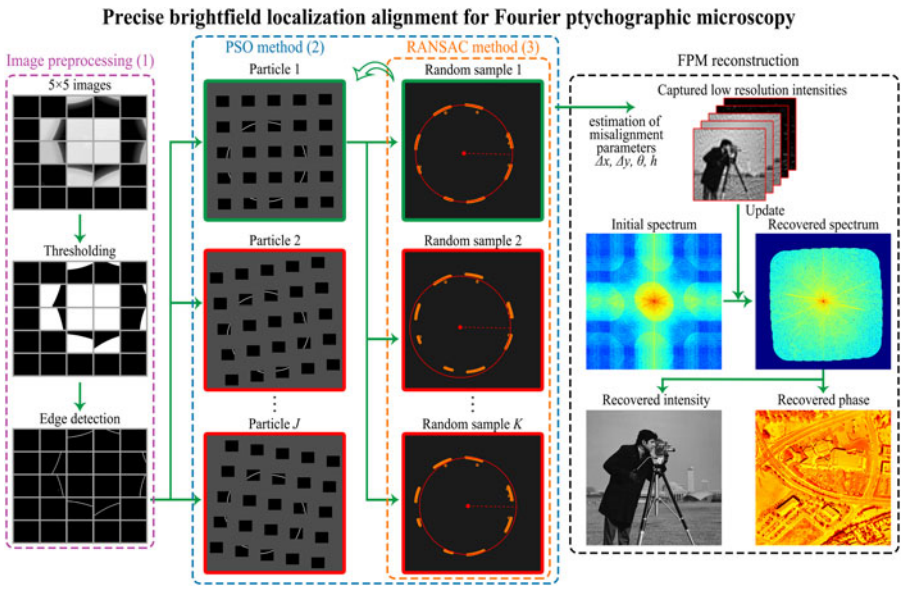

DOI: 10.1109/JPHOT.2017.2780189
1943-0655

Precise Brightfield Localization Alignment for Fourier Ptychographic Microscopy

Jizhou Zhang,[1] **Tingfa Xu**,[1] **Jingdan Liu**,[2] **Sining Chen**,[1] **and Xing Wang**[1]

[1]School of Optoelectronics, Beijing Institute of Technology, Beijing 100081, China
[2]Academy of Opto-Electronics, Chinese Academy of Science, Beijing 100081, China

DOI:10.1109/JPHOT.2017.2780189

Manuscript received October 7, 2017; revised November 13, 2017; accepted December 2, 2017. Date of publication December 6, 2017; date of current version December 25, 2017. This work was supported in part by the Major Science Instrument Program of the National Natural Science Foundation of China under Grant 61527802, and in part by the General Program of the National Natural Science Foundation of China under Grants 61371132 and 61471043. Corresponding authors: Jizhou Zhang and Tingfa Xu (e-mail: 2120140578@bit.edu.cn; ciom_xtf1@bit.edu.cn).

Abstract: Fourier ptychographic microscopy (FPM) is a recently developed microscope technology that overcomes the resolution limit of a low numerical aperture objective lens by employing angular varying illuminations. Combining the concepts of ptychography, synthetic aperture, and phase retrieval, FPM achieves high-resolution, wide-field, and quantitative phase imaging at the same time. In typical FPM systems, the angular varying illuminations are achieved with LED arrays whose positional misalignments bring significant errors in the reconstruction procedure. In previous studies, several LED array alignment methods are developed, which iteratively recover the positional misalignment parameters during the reconstruction. These methods consume additional calculations in FPM reconstruction and may not be practical in other microscopy system. In this work, we represent a preprocessing LED array alignment method by accurately localizing the brightfield area on the sample plane. By applying particle swarm optimization method and random sample consensus method, the global misalignment parameters can be estimated with high accuracy and speed. Both numerical simulations and actual system experiments are carried out to evaluate the effectiveness of our method and the results show that the reconstruction quality of high-resolution images is significantly improved by using our method.

Index Terms: Coherence imaging, microscopy, imaging system.

1. Introduction

Fourier ptychographic microscopy (FPM) is a lately developed technique for high-throughput biomedical observation and quantitative phase imaging [1]–[4]. In FPM, a programmable light emitting diode (LED) array is used to provide oblique plane waves. When the specimen is illuminated by oblique plane waves, high frequency information in Fourier space is shifted into the passband of the objective. Similar to the concept of synthetic aperture [5]–[7], FPM collects images containing high frequency information and stitches them together in Fourier space to enlarge the signal passband of the system. To recover the phase information lost in the acquisition process, FPM also applies a phase retrieval technique [8], [9]. The basic idea of FPM is developed from a lensless imaging method named ptychography [10]–[12] that scans the specimen with a focused beam. The intensity and phase of an illuminated specimen section can be recovered from the diffraction patterns with

phase retrieval methods. Different from ptychography, FPM scans the object spectrum with the objective NA in Fourier space [1]–[4].

Without any mechanical moving components or phase measurements, FPM offers a flexible and low-cost approach to achieve high-resolution, wide-field and quantitative phase imaging. Within a few years, FPM has been applied in many applications such as hematology [13], pathology [14], [15] and quantitative phase imaging [16]. Numerous studies have been implemented lately to improve FPM, including system aberrations correction [17]–[20], rapid acquisition procedure [21]–[24], modified microscope system setup [25]–[28] and the concept of Fourier ptychography even extends to macroscopic imaging [29], [30]. These applications and modifications show the great potential of FPM in biomedical observation and clinical diagnosis. Besides the implementation in FPM, LED arrays have been applied in many other microscopic systems such as differential phase contrast imaging [31] and 3D imaging [32] for their good monochrome, high luminous efficacy and low cost.

In ptychography, a high-quality reconstruction builds on the precise knowledge of the probe scanning positions [10], [33]. Similar to ptychography, the position of the LED array directly affects the reconstruction performance of FPM. Because the incident wave vectors are determined by the relative positions between the LED elements and the sample in FPM. The pcFPM method proposed in [19] can effectively calculate four global positional factors (rotation, horizontal shift and height) of the LED array. However, it needs additional calculation in each iteration, which slows the reconstruction down. Besides, the combination of FPM reconstruction and misalignment correction limits the application on other microscope systems.

In this paper, we propose a preprocessing LED array alignment method termed BFL (brightfield localization). By utilizing the spatial relationship between the LED elements and the brightfield locations on the sample plane, the global misalignment parameters can be estimated. To improve the accuracy and speed, we employ PSO [34] and RANSAC [35] algorithm in this method. Based on FPM theories and the global misalignment model, we achieve the LED array misalignment correction for FPM. Simulations and experiments are carried out to evaluate the effectiveness of our method and the FPM reconstruction results with and without BFL are shown. Both the simulations and experimental results show that the positional misalignment of LED array can be accurately corrected by using BFL and a much higher accuracy is achieved comparing with previous methods.

2. Theories and Methods

2.1 Positional Misalignment in FPM

As shown in Fig. 1(a), a thin specimen $o(\mathbf{r})$ is illuminated with oblique plane waves with wave vectors $\mathbf{u}_l\,(l = 1, 2, \cdots, N_{LED})$ and the optical field exiting the specimen is $e(\mathbf{r}) = o(\mathbf{r})\exp(i2\pi\mathbf{u}_l\mathbf{r})$. The optical field at the aperture plane is the Fourier transform of the exit field, $\mathcal{F}\{e(\mathbf{r})\} = \mathcal{F}\{o(\mathbf{r})\exp(i2\pi\mathbf{u}_l\mathbf{r})\} = O(\mathbf{u} - \mathbf{u}_l)$, where $\mathbf{u} = (f_x, f_y)$ represents the 2D frequency coordinates in Fourier domain. With the optical field low-pass filtered by the objective pupil function $P(\mathbf{u})$, the complex fields at the image plane can be expressed as

$$g_{le}(\mathbf{r}) = \mathcal{F}^{-1}\left\{P(\mathbf{u})O(\mathbf{u} - \mathbf{u}_l)\right\} \tag{1}$$

which is the forward model of FPM.

By reversing the forward model of FPM, the reconstruction process synthesizes sub-spectrums corresponding to different illumination angles into a higher throughput spectrum. However, the phase information is lost when the image sensor records the intensities. For this reason, the sub-spectrums cannot be synthesized directly like synthetic aperture methods. To recover the lost phase information from captured intensity images, various phase-retrieval algorithms are introduced into FPM. Most algorithms solve the FPM problem by minimizing the difference between the measured and estimated amplitudes (or intensities), formulated as

$$\min_{O(\mathbf{u})} \epsilon = \min_{O(\mathbf{u})} \sum_{l} \sum_{\mathbf{r}} \left| \sqrt{I_{lc}(\mathbf{r})} - \left| g_{le}(\mathbf{r}) \right| \right|^2 \tag{2}$$

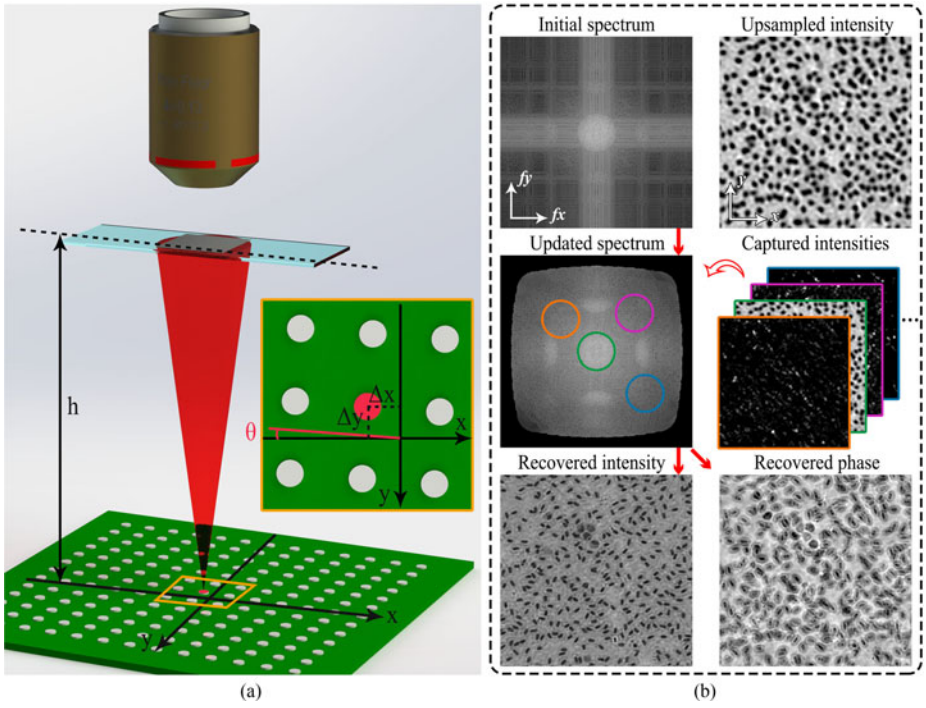

Fig. 1. The basic concept of FPM. (a) The system setup of FPM. (b) The reconstruction procedure of FPM.

where $I_{lc}(\mathbf{r})$ is the low resolution intensity images recorded by the camera. As shown in Fig. 1(b), the most common strategy is to replace the estimated amplitudes with the measured amplitudes, which can be formulated as

$$O^{u}(\mathbf{u}-\mathbf{u}_l) = P(\mathbf{u})\mathcal{F}\left\{\frac{\left|\sqrt{I_{lc}(\mathbf{r})}\right|}{|g_{le}(\mathbf{r})|}g_{le}(\mathbf{r})\right\} \tag{3}$$

where $O^{u}(\mathbf{u}-\mathbf{u}_l)$ is the updated sub-spectrum. At last, by transforming the spectrum back to the spatial domain, the high-resolution intensity and phase are extracted.

In FPM, the wave vectors of oblique plane waves are determined by the positions of LED elements so that the accuracy of LED positions directly affects the quality of FPM reconstruction results. When non-negligible misalignment exists, there will be significant errors in recovered intensity and phase. A comparison of simulated FPM reconstruction results with and without positional misalignment is shown in Fig. 2. The ideal LED positions are labeled with blue X marks and the actual LED positions are labeled with orange dots in Fig. 2(a). Fig. 2(b) and (c) show the recovered intensity and phase of FPM with and without misalignment respectively. It can be observed that the positional misalignment introduces significant errors into the recovered high-resolution intensity and phase.

Typically, the LED array can be regarded as a rigid object and the LED elements are uniformly placed on the array. So that we can build a global misalignment model and the positional deviation of each LED element can be directly calculated from the global model. The global misalignment of LED array in FPM can be modeled with four parameters that are shift factors along x-axis and y-axis Δx, Δy, rotation factor θ and height factor h. The magnified area in Fig. 1(a) shows the misalignment parameters of LED array in FPM. The red LED is in central position of the array and corresponding to 0 row, 0 column. The position of each LED element can be expressed as

$$\begin{bmatrix} x_{m,n} & y_{m,n} \end{bmatrix} = \begin{bmatrix} nd & md \end{bmatrix} \cdot \begin{bmatrix} \cos\theta & \sin\theta \\ -\sin\theta & \cos\theta \end{bmatrix} + \begin{bmatrix} \Delta x & \Delta y \end{bmatrix} \tag{4}$$

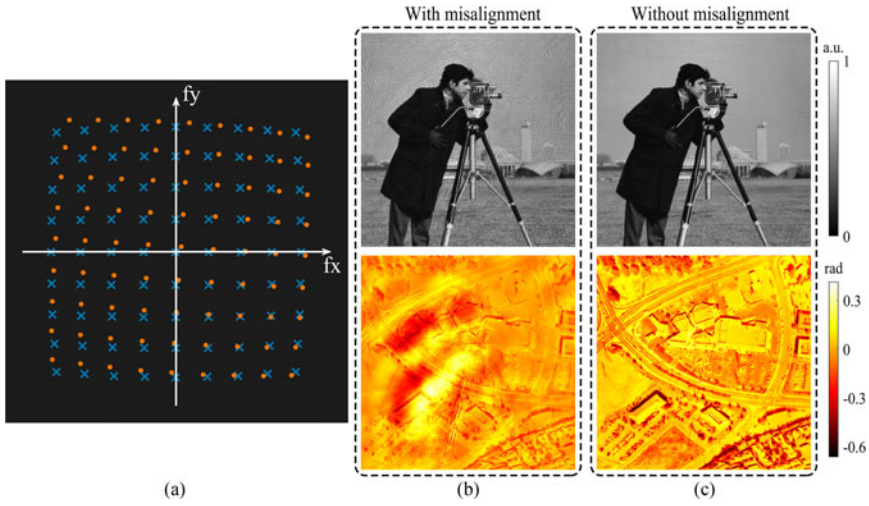

Fig. 2. The positional misalignment in FPM. (a) shows the aperture positions corresponding to different oblique plane waves in Fourier domain. (b) represents the recovered intensity and phase of FPM when positional misalignment exists. (c) shows the recovered results when no misalignment exists.

where m, n present different rows and columns of the array ($m, n = -2, -1, \cdots, 2$) and d is the distance between adjacent LED elements. The wave vector of each LED element can be formulated as

$$\begin{bmatrix} f_x & f_y \end{bmatrix} = -\frac{2\pi}{\lambda \cdot \sqrt{(x_{m,n} - \Delta x)^2 + (y_{m,n} - \Delta y)^2 + h^2}} \cdot \begin{bmatrix} x_{m,n} - \Delta x & y_{m,n} - \Delta y \end{bmatrix} \tag{5}$$

Once the misalignment parameters are corrected, the reconstruction performance can be significantly improved.

2.2 LED Array Precise Alignment With Brightfield Localization (BFL)

In conventional FPM, the LED array is considered to be sufficiently far from the specimen, so that the illumination of each LED is approximately a plane wave from a specific angle. For a small region of interest in the specimen, this assumption is accurate enough for the algorithm to reconstruct a complex field of the region. But in a large field of view (FOV), the size of the specimen cannot be ignored comparing with the illumination distance. Accordingly, each position in the specimen has a different illumination angle, as shown in Fig. 1(a). The pixel lies in the brightfield when the corresponding illumination NA (sinusoidal value of the illumination angle) is less than the objective NA and in the darkfield when the corresponding illumination NA is larger. As a result, the ideal brightfield shape of a LED element should be a shifted circle, as shown in Fig. 1(a). If the brightfield of each LED element can be measured, the LED array can be easily aligned. However, the brightfield area is larger than the imaging area of the detector in most microscope systems. To locate the whole brightfield of a LED elemtent, we can either dicrease the distance between the LED and the sample plane or shift the LED horizontally and stitch images together to enlarge the equivalent imaging area. In condition of the periodic repetition of the LED array, it is possible to combine several images corresponding to neighboring LEDs and enlarge the sampling area of illumination angle.

In the experimental setup of our FPM system, we stitch the information corresponding to 25 LEDs (5 rows, 5 columns) to calculate the accurate misalignment parameters of the LED array, because this offers a large enough searching area and requires little calculation. No specimen is placed on the stage when corresponding images are captured so that the brightfield can be precisely localized in the images. The edge points of the brightfield are used to locate the brightfield because this reduces calculation and edge points are easy to locate. Using geometric transformation, all

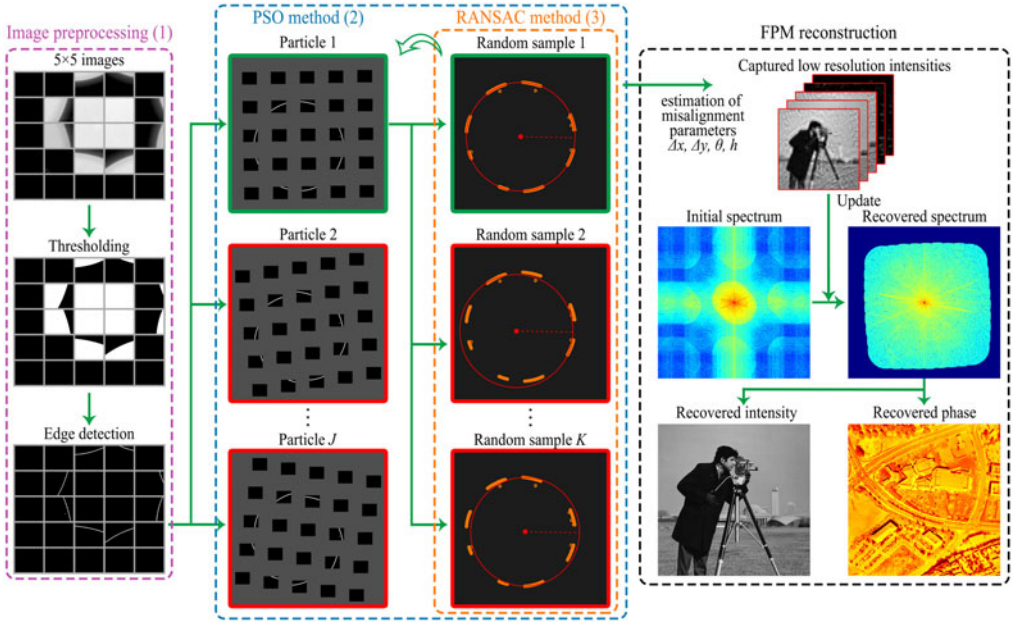

Fig. 3. The flow diagram of applying BFL in FPM reconstruction. The BFL include three steps that are preprocessing, PSO method and RANSAC method.

edge points in these images are combined into one coordinate which is the object plane of the central LED. The position of each edge point on the object plane can be expressed as

$$\begin{bmatrix} px' & py' \end{bmatrix} = -\frac{1}{\beta}\left(\begin{bmatrix} px_{m,n} & py_{m,n} \end{bmatrix}\right) - \begin{bmatrix} nd & md \end{bmatrix} \cdot \begin{bmatrix} \cos\theta & \sin\theta \\ -\sin\theta & \cos\theta \end{bmatrix} \tag{6}$$

where $px_{m,n}$ and $py_{m,n}$ are the original positions on the image plane corresponding to different images, β is the magnification of the objective lens. Afterwards, the misalignment estimate problem is translated into an optimization problem which is to find the best parameters to model the brightfield circle, formulated as

$$\left(\widehat{\Delta x}, \widehat{\Delta y}, \widehat{\theta}, \widehat{h}\right) = \arg \max_{\Delta x, \Delta y, \theta, h} \sum P\left(px', py'\right), \quad \left(px' \in \mathbf{px}', py' \in \mathbf{py}'\right) \tag{7}$$

$$P\left(x, y\right) = \begin{cases} 1, & \text{if } \left|\sqrt{(x+\Delta x)^2 + (y+\Delta y)^2} - R\right| < th \\ 0, & \text{otherwise} \end{cases} \tag{8}$$

$$R = h \cdot \tan\left(\arcsin\left(\mathrm{NA}\right)\right) \tag{9}$$

where $\widehat{\Delta x}$, $\widehat{\Delta y}$, $\widehat{\theta}$ and $\widehat{h}$ are the estimation of the actual misalignment parameters, $\mathbf{px}'$ and $\mathbf{py}'$ are the collection of positons of all edge points, R is the radius of the estimated circle and th is the distance threshold. The function $P\left(x, y\right)$ in (8) distinguishes whether the edge point is on the estimated brightfield circle or not. As long as the distance between the edge point and the circle centered in $(-\Delta x, -\Delta y)$ is less than the predefined threshold th, the edge point is considered to be on the estimated brightfield circle. By maximizing the number of edge points on the estimated brightfield circle, the global misalignment parameters Δx, Δy, θ and the radius R can be estimated. The last misalignment parameter h can be calculated using R and the objective NA. In fact, the optimization problem defined in (6)–(9) is rather tough to solve with numerical solutions. Under the assumption that the global misalignment model is valid, the accurate solution can be regarded as a point in a four-dimensional continuous space defined by four misalignment parameters. Therefore, we can use optimization search method to find the approximate solution in a predefined support domain

Algorithm 1: Brightfield localization (BFL).

Input: 25 Images corresponding to the central 25 LEDs;
Output: The estimation of misalignment parameters $\widehat{\Delta x}$, $\widehat{\Delta y}$, $\widehat{\theta}$ and $\widehat{h}$;
Step 1: Image preprocessing
Use the Otsu algorithm to segment the image;
Use the Canny opeartor to detect all edge points;
Record the positions on the image plane of all edge points;
Step 2: PSO algorithm
Initialize J particles. Each partlcle has a random estimate θ_j;
for $i = 1$ to $N_{iteration}$ **do**
  for $j = 1$ to J **do**
    Calculate the positions on the object plane of all edge points with θ_j;
    Step 3: RANSAC algorithm
    for $k = 1$ to K **do**
      Randomly select 3 edge points.
      Calculate the circle parameters $\left(-\widehat{\Delta x_k}, -\widehat{\Delta y_k}\right)$ and $\widehat{R_k}$ determined by these points ;
      Calculate the value of the function $P(x, y)$;
      Record the parameters corresponding to the largest fitness in all RANSAC sampling;
    end for
    Record the parameters of all PSO particles in one iteration;
  end for
  Record the parameters of all PSO particles in all iteration;
  Update the estimation $\theta_j (j = 1, 2, ..., J)$ and speed of all particles according to the fitness of all PSO particles in all iteration;
end for
Pick up the best estimation $\widehat{\Delta x}$, $\widehat{\Delta y}$, $\widehat{\theta}$ and $\widehat{h}$ corresponding to the largest fitness.

of all misalignment parameters. As long as the misalignment parameters are within the support domain and the optimization search method is effective, we can reach an accurate enough solution to correct the misalignment. Specifically, we divide this optimization search problem into two parts for the consideration of speed and accuracy. Part one is the searching of θ and part two is the estimation of Δx, Δy and h. Given an estimation of θ, the positions of edge points on the object plane are defined, then the estimation of Δx, Δy and h can be reached by fitting the brightfield circle with the edge points. So that, the part two is actually embedded into part one. To solve the problem of part one and part two, we use two optimization algorithm RANSAC and PSO. RANSAC is an iterative method to quickly estimate parameters of a mathematical model from a set of observed data that contains outliers. Since there are thousands of edge points, containing hundreds of outlers, RANSAC is very suitable for estimating the parameters of the brightfield circle. PSO method is a kind of evolutionary algorithm to search the global optimal solution quickly and precisely with a predefined fitness. Hence, we use PSO algorithm to search the approximate solution of θ. The fitness of RANSAC is the value of the function $P(x, y)$ and the fitness of PSO is the fitness of the best RANSAC estimation. We name the method that aligns LED array with brightfield localization, RANSAC algorithm and PSO algorithm as the BFL method. With the nested iteration of PSO algorithm and RANSAC algorithm, an accurate enough solution of the misalignment parameters is achieved. As the pixel size is of several microns, the accuracy of estimated parameters is at the micron level. The detailed processes of BFL are listed in **Algorithm 1** and the flow diagram of BFL is shown in Fig. 3.

The misalignment parameters can be reached with BFL and used to perform the FPM reconstruction. The rotation $\widehat{\theta}$ and the shift factors $\widehat{\Delta x}$, $\widehat{\Delta y}$ is directly calculated during the PSO iterations while the height factor $\widehat{h}$ can be calculated with circumcircle radius $\widehat{R}$ and the objective NA. With all misalignment parameters imported into the global misalignment model, the positions of all LED

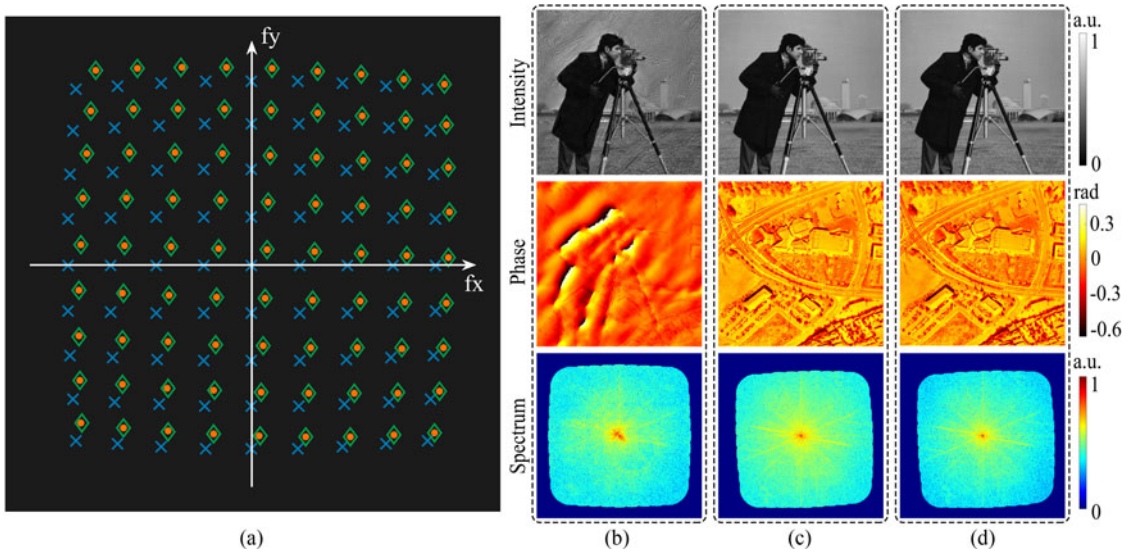

Fig. 4. An example of positional misalignment correction with BFL. (a) shows the corresponding positions of three LED position sets in Fourier domain. (b) represents the recovered results of FPM when positional misalignment exists. (c) shows the recovered results corrected with BFL. (d) shows the recovered results corrected with the actual misalignment parameters.

elements can be corrected. Applying the corrected LED positions, a more accurate reconstruction can be performed.

3. Experiment Results

3.1 The Effectiveness and Robustness of BFL Under Noise

We first validate BFL using numerical simulations before implementing it to an experimental system. The simulation parameters are carefully chosen to model a real FPM system, with an incident wavelength of 629 nm, 2160 $\times$ 2560 imaging pixels of 6.5 μm size and a 4$\times$ objective of 0.13 NA. We simulate sets of images with different misalignment and noise levels and apply BFL on these image sets to correct the misalignment. The root-mean-squared errors (RMSE) between the estimated misalignment parameters and the real parameters are recorded to quantitatively evaluate the effectiveness and robustness of BFL. The simulations are carried out on a personal computer equipped with an Intel i7-6700K CPU, 16 GB DDR4 memory. The numerical calculation software we use is Matlab 2016b which is installed on a Windows 10 operating system.

Fig. 4 is an example of our numerical simulation. Fig. 4(a) shows the aperture positions corresponding to different LED elements. The uncorrected positions with predefined misalignment are labeled with blue X marks, the actual positions are labeled with green diamonds and the corrected positions are labeled with orange dots. The reconstruction results corresponding to these three set of LED positions are shown in Fig. 4(b)–(d) respectively. The simulation results indicate that the LED array can be accurately aligned with BFL and the FPM reconstruction results are significantly improved after the correction.

To numerically analyze the effectiveness and robustness of BFL, we test the performance of BFL under different noise levels. Brightfield or darkfield images are generated based on the positional relationship between the LED array and the specimen. White Gaussian noises with the noise standard deviation $\sigma = 0, 0.01, 0.02, 0.04, 0.08$ are added to the simulated images. Under each noise condition, 100 random positional misalignments are simulated and the RMSE of the BFL estimated misalignment parameters $(\Delta x, \Delta y, \theta, h)$ are recorded, as shown in Fig. 5. Limits are set to the range of simulated positional misalignment parameters as $\Delta x \in [-3000\,\mu\text{m}, 3000\,\mu\text{m}]$,

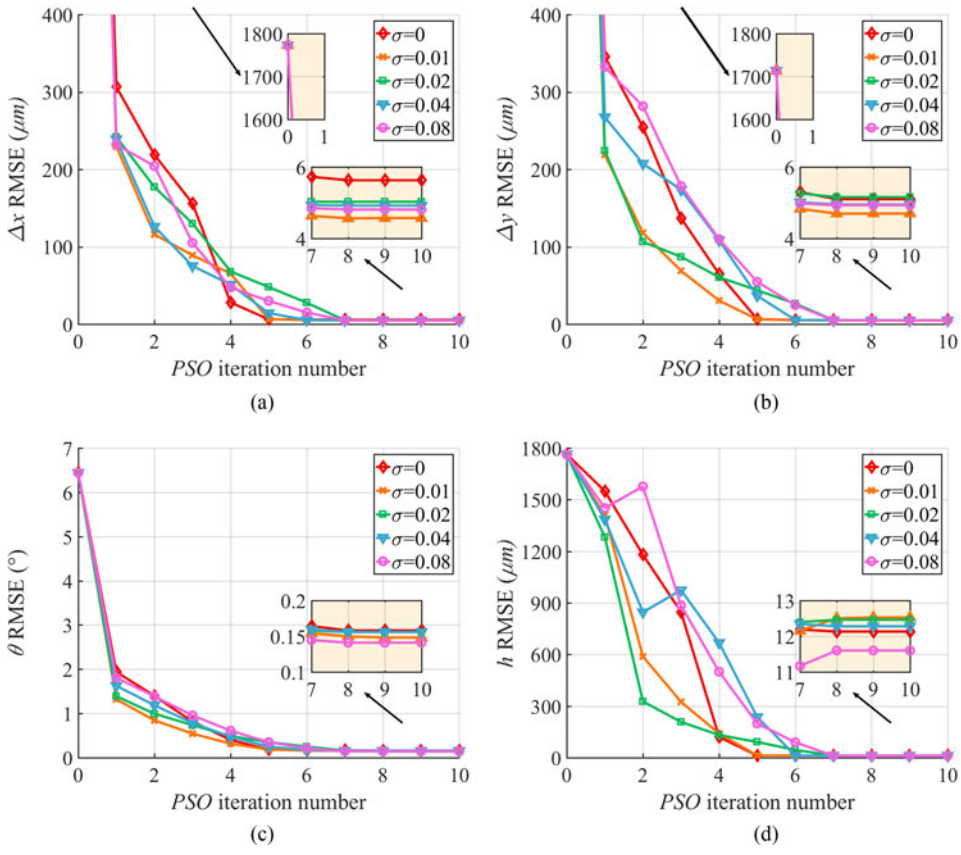

Fig. 5. The performance of BFL under different noise conditions. (a)–(d) show the RMSE of four position factors (Δx, Δy, θ, h) during iterations of BFL with standard deviation $\sigma = 0, 0.01, 0.02, 0.04, 0.08$.

TABLE 1
The RMSE of BFL Misalignment Estimation Under Different Noise Conditions

Parameter	RMSE under different noise standard deviation θ				
	0	0.01	0.02	0.04	0.08
$\Delta x(\mu$m)	5.63	4.57	5.03	4.92	4.81
$\Delta y(\mu$m)	5.10	4.70	5.16	4.95	4.93
$\theta(^\circ)$	0.16	0.15	0.16	0.16	0.14
$h(\mu$m)	12.13	12.53	12.46	12.28	11.60

$\Delta y \in [-3000\,\mu\text{m}, 3000\,\mu\text{m}]$, $\theta \in [-10^\circ, 10^\circ]$ and $h \in [-3000\,\mu\text{m}, 3000\,\mu\text{m}]$. In a real experimental condition, the LED array can be easily aligned manually to insure that the positional misalignment parameters are within the limits so that the BFL is able to correct the misalignment. Table 1 shows the RMSE of estimation of four misalignment parameters under different noise levels using BFL.

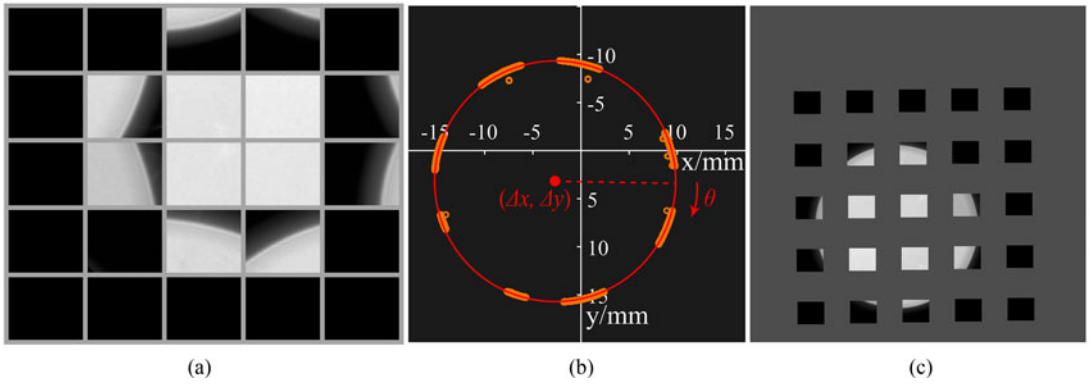

Fig. 6. Positional misalignment correction with 55 images. (a) The intensity images corresponding to the central 55 LEDs. (b) The edge points combined into the same coordinate and the estimated brightfield boundary. (c) The combined image using the estimated parameters.

As shown in Fig. 5 and Table 1, the misalignment parameters can be precisely estimated even when severe noises exist. This is because that the estimation accuracy of BFL only depends on the positional accuracy of detected edge points and the edge points can still be precisely located under severe noises. As a contrast, the pcFPM method proposed in Reference [19] is seriously affected by noise and its accuracy decreases by one to two orders of magnitude when severe noises exist. Besides, BFL method is not very sensitive to the size of searching area for the reason that Δx, Δy and h are directly estimated using RANSAC method rather than searching in a predefined range. Comparing with the simulation in Reference [19], the BFL method corrects the misalignment in a much larger area and the calculation only costs less than 10 s. In summary, the simulation results show that BFL offers an accurate, fast and robust approach to detect and correct the positional misalignment of the LED array and the FPM reconstruction performance can be significantly improved with BFL.

3.2 The Implement of BFL on a FPM System

To evaluate the validity of BFL experimentally, we correct the global misalignment of a real FPM system with BFL and compare the reconstruction result with and without BFL. The experimental microscope system is modified from a biological microscope and equipped with a 4$\times$ objective of 0.13 NA. A scientific CMOS (sCMOS) camera with 2560 $\times$ 2160 pixels (6.5 μm pixel size) is used for FPM intensity capture. We place a customized 13 $\times$ 13 LED array (8.128 mm interval) 100 mm below the specimen for providing angle-varied illumination (629 nm central wavelength). The field of the system is 16.64 mm $\times$ 14.04 mm and the equivalent NA of the FPM reconstruction result is about 0.7. The LED is manually aligned before applying BFL and the LED array misalignment is in the same range with simulations. All images are recorded with 100 ms exposure time and a noise suppression operation is applied to all images.

Before capturing the intensity images for FPM reconstruction, the intensity images corresponding to the central 5 $\times$ 5 LEDs without specimens on the stage are captured, as shown in Fig. 6(a). The positional misalignment parameters of the LED array are estimated using the 5 $\times$ 5 images with BFL. All edge points in these images are combined into the same coordinate and labeled with little orange hollow circles in Fig. 6(b). The red circle shown in Fig. 6(b) is the brightfield boundary estimated with BFL. Fig. 6(c) shows the combined image in the object space using the estimated parameters. Afterwards, corrected positions of all LEDs can be calculated with the global misalignment model. With the application of PSO and RANSAC algorithms, the global misalignment parameters can be estimated with high accuracy and speed.

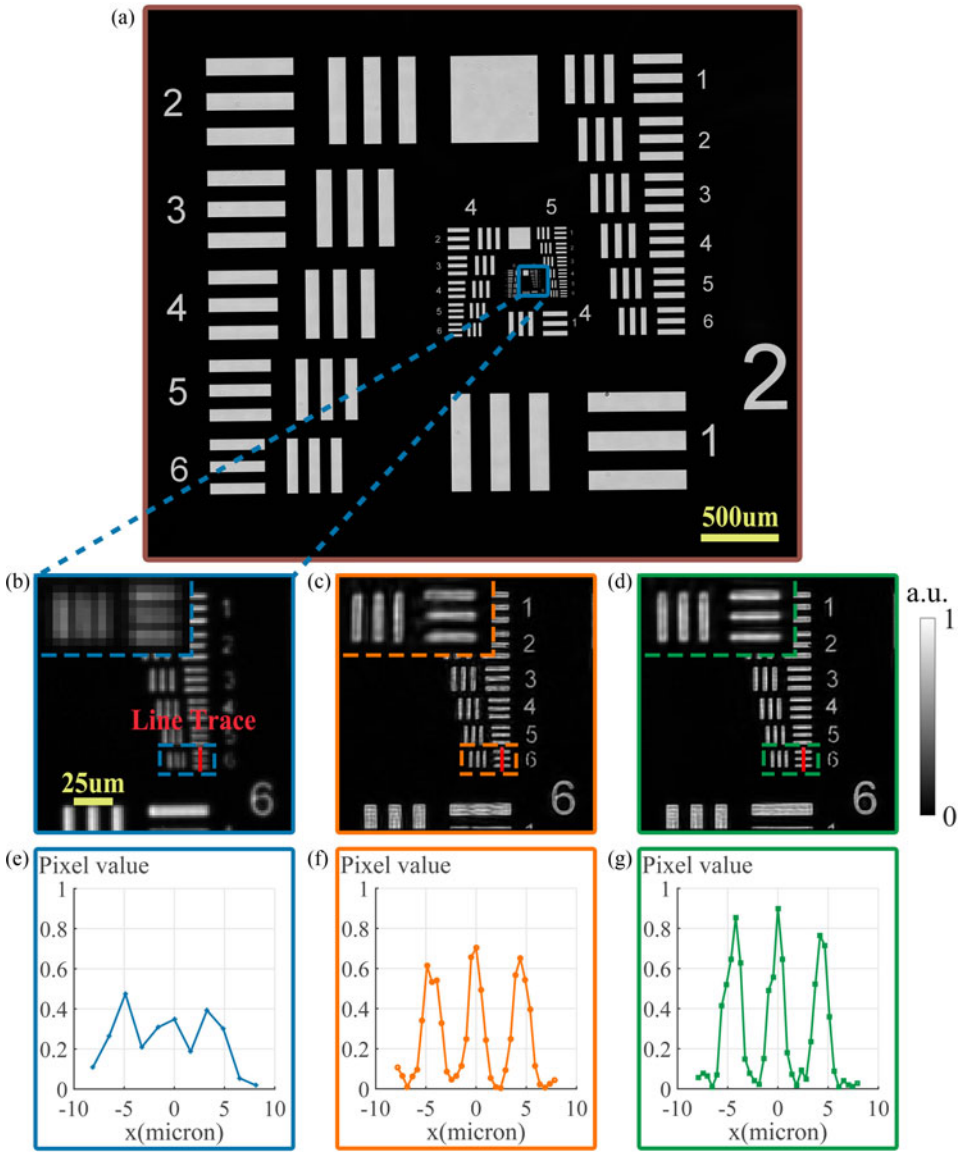

Fig. 7. Reconstruction result of a USAF target segment. (a) The low resolution intensity image. (b) The magnified ROI in (a). (c) The recovered ROI with uncorrected LED positions. (d) The recovered ROI with corrected LED positions using BFL. (e)–(g) The line traces of the resolution target image corresponding to (b)–(d).

We compare the recovered intensity of a USAF target segment with the uncorrected LED positions and corrected LED positions using BFL. Fig. 7(a) presents the low resolution image of the resolution target and a magnified region of interest (ROI) is shown in Fig. 7(b). Fig. 7(c) and (d) are the recovered intensity images of the region with uncorrected and corrected LED positions. Fig. 7(e) and (f) show the intensity line traces of the resolution target corresponding to Fig. 7(b)–(d). The high-resolution complex field of the ROI is recovered with 169 intensity image sections of 100 $\times$ 100 pixels and the recovered size is 350 $\times$ 350 pixels with equivalent 0.7 NA. More details, higher contrast and fewer distortions are achieved with BFL. With the application of BFL, the positional misalignment parameters are efficiently estimated and the reconstruction quality is significantly improved.

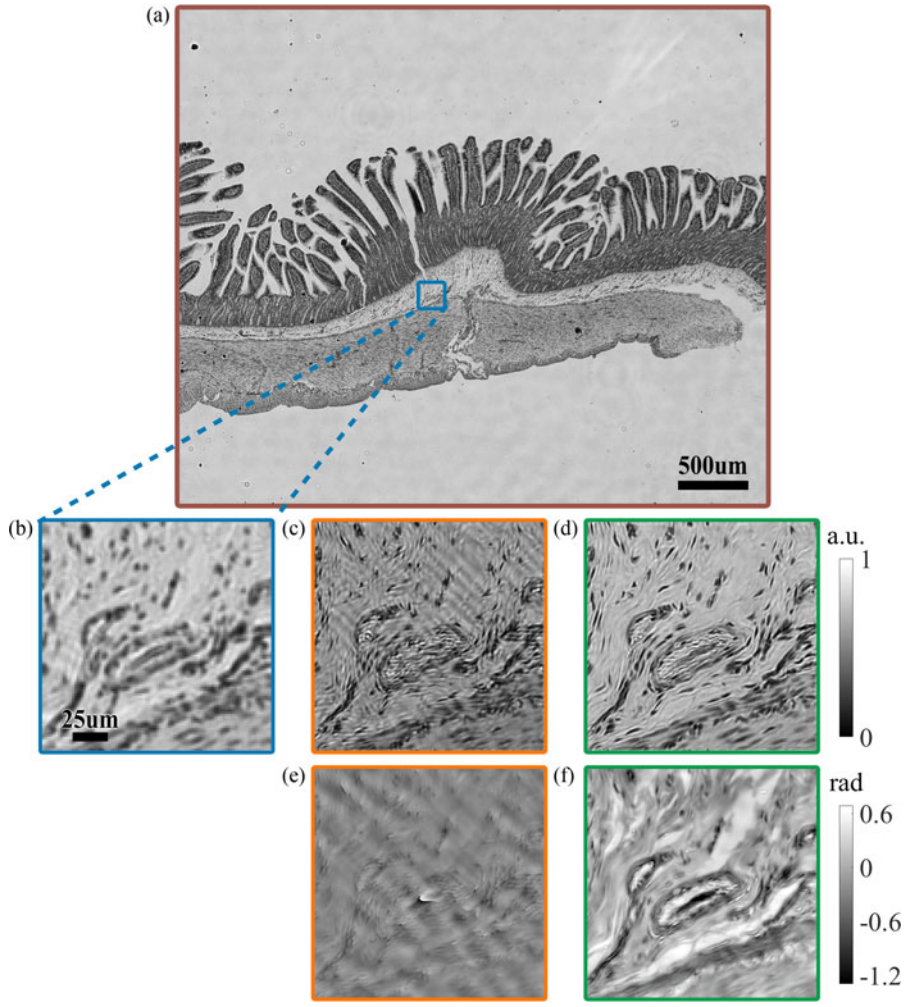

Fig. 8. Reconstruction result of an animal intestine tissue segment. (a) The low resolution intensity image. (b) The magnified region of interest (ROI) in (a). (c) The recovered ROI with uncorrected LED positions. (d) The recovered ROI with corrected LED positions using BFL. (e)-(f) The recovered phase corresponding to (c)-(d).

The reconstruction performances of an animal intestine tissue with uncorrected LED positions and corrected LED positions using BFL are also compared. Fig. 8(a) shows the whole FOV of the specimen and a ROI is magnified in Fig. 8(b). Fig. 8(c) and (d) are the recovered intensity images of the ROI with uncorrected and corrected LED positions. The recovered phase images are shown in Fig. 8(e) and (f). It can be observed that the reconstruction results with uncorrected LED positions are obviously distorted because of the positional misalignment. With the help of BFL, the distortions in the results are removed and a high quality reconstruction result is reached.

4. Conclusion

In this paper, we have proposed a preprocessing LED array alignment method named BFL for FPM reconstruction with brightfield localization. The basic idea of BFL is to locate the brightfield of the central LED elements by utilizing the relationship between the brightfield positions and the illumination angles. With the PSO and RANSAC algorithms, the positional parameters can be reached with high accuracy and speed. To quantitatively analyze the performance of BFL, we generate

randomly selected misalignment parameters under different noise level and use BFL to estimate the misalignment parameters. The simulations show that BFL can accurately correct the misalignment of the LED array even in severe noise condition and the FPM reconstruction is significantly improved with BFL. We also build an experimental FPM system to validate the effectiveness of BFL. Experiments show that the LED array is precisely aligned and the reconstruction quality of high-resolution images is significantly improved by applying BFL. Different from previously developed methods that iteratively recover the global positional parameters during FPM reconstruction, BFL method calculate these parameters in a preprocessing step. This makes it possible to apply BFL to any microscope system that uses a LED array as illuminations. In conclusion, the BFL method is a flexible and effective method to accurately align the LED array in FPM or other microscope system. It will promote the practical use of FPM in biomedical observation and clinical diagnosis.

In addition, BFL method is based on the fact that the illumination NA is not the same in different regions of the specimen. In other words, the size of the specimen cannot be ignored comparing with the illumination distance. The differences of illumination NA decrease the reconstruction results of FPM because FPM assumes the illumination NA does not change in a single image. It will be a future work for us to build a model to describe the illumination difference for FPM and try to improve the reconstruction results.

Acknowledgment

The authors wish to thank the anonymous reviewers for their valuable suggestions.

References

[1] G. Zheng, R. Horstmeyer, and C. Yang, "Wide-field, high-resolution Fourier ptychographic microscopy," *Nature Photon.*, vol. 7, no. 9, pp. 739–745, Jul. 2013.
[2] G. Zheng, "Breakthroughs in photonics 2013: Fourier ptychographic imaging," *IEEE Photon. J.*, vol. 6, no. 2, Apr. 2014, Art. no. 0701207.
[3] X. Ou, R. Horstmeyer, G. Zheng, and C. Yang, "High numerical aperture Fourier ptychography: Principle, implementation and characterization," *Opt. Express*, vol. 23, no. 3, pp. 3472–3491, 2015.
[4] K. Guo, S. Dong, and G. Zheng, "Fourier ptychography for brightfield, phase, darkfield, reflective, multi-slice, and fluorescence imaging," *IEEE J. Sel. Topics Quantum Electron.*, vol. 22, no. 4, Jul./Aug. 2016, Art. no. 6802712.
[5] T. M. Turpin, L. H. Gesell, J. Lapides, and C. H. Price, "Theory of the synthetic aperture microscope," *Proc. SPIE, Adv. Imag. Technol. Commercial Appl.*, vol. 2566, pp. 230–240, Aug. 1995.
[6] V. Mico, Z. Zalevsky, P. García-Martínez, and J. García, "Synthetic aperture superresolution with multiple off-axis holograms," *J. Opt. Soc. Amer. A*, vol. 23, no. 12, pp. 3162–3170, 2006.
[7] T. R. Hillman, T. Gutzler, S. A. Alexandrov, and D. D. Sampson, "High-resolution, wide-field object reconstruction with synthetic aperture Fourier holographic optical microscopy," *Opt. Express*, vol. 17, no. 10, pp. 7873–7892, 2009.
[8] J. R. Fienup, "Phase retrieval algorithms: A comparison," *Appl. Opt.*, vol. 21, no. 15, pp. 2758–2769, 1982.
[9] A. M. Maiden and J. M. Rodenburg, "An improved ptychographical phase retrieval algorithm for diffractive imaging," *Ultramicroscopy*, vol. 109, no. 10, pp. 1256–1262, 2009.
[10] J. M. Rodenburg and R. H. T. Bates, "The theory of super-resolution electron microscopy via Wigner-distribution deconvolution," *Philos. Trans. Phys. Sci. Eng.*, vol. 339, no. 1655, pp. 521–553, 1992.
[11] H. M. Faulkner and J. M. Rodenburg, "Movable aperture lensless transmission microscopy: A novel phase retrieval algorithm," *Phys. Rev. Lett.*, vol. 93, no. 2, 2004, Art. no. 023903.
[12] J. M. Rodenburg *et al.*, "Hard-X-ray lensless imaging of extended objects," *Phys. Rev. Lett.*, vol. 98, no. 3, pp. 17–21, 2007.
[13] J. Chung, X. Ou, R. P. Kulkarni, and C. Yang, "Counting white blood cells from a blood smear using fourier ptychographic microscopy," *PLoS One*, vol. 10, no. 7, 2015, Art. no. e0133489.
[14] R. Horstmeyer, X. Ou, G. Zheng, P. Willems, and C. Yang, "Digital pathology with Fourier ptychography," *Comput. Med. Imag. Graph.*, vol. 42, pp. 38–43, 2015.
[15] A. Williams *et al.*, "Fourier ptychographic microscopy for filtration-based circulating tumor cell enumeration and analysis," *J. Biomed. Opt.*, vol. 19, no. 6, 2014, Art. no. 066007.
[16] X. Ou, R. Horstmeyer, C. Yang, and G. Zheng, "Quantitative phase imaging via Fourier ptychographic microscopy," *Opt. Lett.*, vol. 38, no. 22, pp. 4845–4848, 2013.
[17] C. Zuo, J. Sun, and Q. Chen, "Adaptive step-size strategy for noise-robust Fourier ptychographic microscopy," *Opt. Express*, vol. 24, no. 18, pp. 20724–20744, 2016.
[18] X. Ou, G. Zheng, and C. Yang, "Embedded pupil function recovery for Fourier ptychographic microscopy," *Opt. Express*, vol. 22, no. 5, pp. 4960–4972, 2014.
[19] J. Sun, Q. Chen, Y. Zhang, and C. Zuo, "Efficient positional misalignment correction method for Fourier ptychographic microscopy," *Biomed. Opt. Express*, vol. 7, no. 4, pp. 1336–1350, Apr. 2016.

[20] R. Horstmeyer, R. Y. Chen, X. Ou, B. Ames, J. A. Tropp, and C. Yang, "Solving ptychography with a convex relaxation," *New J. Phys.*, vol. 17, no. 5, 2015, Art. no. 53044.
[21] L. Bian, J. Suo, G. Situ, G. Zheng, F. Chen, and Q. Dai, "Content adaptive illumination for Fourier ptychography," *Opt. Lett.*, vol. 39, no. 23, pp. 6648–6651, 2014.
[22] S. Dong, R. Shiradkar, P. Nanda, and G. Zheng, "Spectral multiplexing and coherent-state decomposition in Fourier ptychographic imaging," *Biomed. Opt. Express*, vol. 5, no. 6, pp. 1757–1761, 2014.
[23] J. Sun *et al.*, "Coded multi-angular illumination for Fourier ptychography based on Hadamard codes," in *Proc. SPIE, Int. Conf. Opt. Photon. Eng.*, vol. 9524, Jul. 2015, Paper 95242C.
[24] L. Tian, X. Li, K. Ramchandran, and L. Waller, "Multiplexed coded illumination for Fourier ptychography with an LED array microscope," *Biomed. Opt. Express*, vol. 5, no. 7, pp. 2376–2389, 2014.
[25] S. Dong, K. Guo, P. Nanda, R. Shiradkar, and G. Zheng, "FPscope: A field-portable high-resolution microscope using a cellphone lens," *Biomed. Opt. Express*, vol. 5, no. 10, pp. 3305–3310, 2014.
[26] K. Guo, Z. Bian, S. Dong, P. Nanda, Y. M. Wang, and G. Zheng, "Microscopy illumination engineering using a low-cost liquid crystal display," *Biomed. Opt. Express*, vol. 6, no. 2, pp. 574–579, 2015.
[27] W. Luo, A. Greenbaum, Y. Zhang, and A. Ozcan, "Synthetic aperture-based on-chip microscopy," *Light, Sci. Appl.*, vol. 4, no. 3, 2015, Art. no. e261.
[28] S. Pacheco, G. Zheng, and R. Liang, "Reflective Fourier ptychography," *J. Biomed. Opt.*, vol. 21, no. 2, 2016, Art. no. 026010.
[29] S. Dong *et al.*, "Aperture-scanning Fourier ptychography for 3D refocusing and super-resolution macroscopic imaging," *Opt. Express*, vol. 22, no. 11, pp. 13586–13599, 2014.
[30] J. Holloway *et al.*, "Toward long-distance subdiffraction imaging using coherent camera arrays," *IEEE Trans. Comput. Imag.*, vol. 2, no. 3, pp. 251–265, Sep. 2016.
[31] Z. Liu, L. Tian, S. Liu, and L. Waller, "Real-time brightfield, darkfield, and phase contrast imaging in a light-emitting diode array microscope," *J. Biomed. Opt.*, vol. 19, no. 10, 2014, Art. no. 106002.
[32] L. Tian and L. Waller, "3D intensity and phase imaging from light field measurements in an LED array microscope," *Optica*, vol. 2, no. 2, pp. 104–111, 2015.
[33] A. Shenfield and J. M. Rodenburg, "Evolutionary determination of experimental parameters for ptychographical imaging," *J. Appl. Phys.*, vol. 109, 2011, Art. no. 124510.
[34] J. Kennedy and R. Eberhart, "Particle swarm optimization," in *Proc. Int. Conf. Neural Netw.*, vol. 4, 1995, pp. 1942–1948.
[35] M. A. Fischler and R. C. Bolles, "Random sample consensus: A paradigm for model fitting with applications to image analysis and automated cartography," *Commun. ACM*, vol. 24, no. 6, pp. 381–395, 1981.